NeuroImage 233 (2021) 117961

Contents lists available at ScienceDirect

NeuroImage

journal homepage: www.elsevier.com/locate/neuroimage

Estimation of the net influx rate K_i and the cerebral metabolic rate of glucose MR_{glc} using a single static [^{18}F]FDG PET scan in rats

Daniele Bertoglio[a], Steven Deleye[a], Alan Miranda[a], Sigrid Stroobants[a,b], Steven Staelens[a], Jeroen Verhaeghe[a,*]

[a] Molecular Imaging Center Antwerp (MICA), University of Antwerp, Antwerp, Belgium
[b] Nuclear Medicine Department, University Hospital Antwerp, Antwerp, Belgium

ARTICLE INFO

Keywords:
Brain
FDG
Glucose
PET
Rat
Body weight
Dynamic imaging
Quantification

ABSTRACT

Since accurate quantification of 2-deoxy-2–^{18}F-fluoro-D-glucose ([^{18}F]FDG) positron emission tomography (PET) requires dynamic acquisition with arterial input function, more practical semi-quantitative (static) approaches are often preferred. However, static standardized uptake values (SUV) are typically biased due to large variations in body weight (BW) occurring over time in animal studies. This study aims to improve static [^{18}F]FDG PET SUV quantification by better accounting for BW variations in rats. We performed dynamic [^{18}F]FDG PET imaging with arterial blood sampling in rats ($n = 27$) with different BW (range 0.230–0.487 kg). By regressing the area under the curve of the input function divided by injected activity against BW (r^2=0.697), we determined a conversion factor f(BW) to be multiplied with SUV and SUV_{glc} to obtain ratSUV and $ratSUV_{glc}$, providing an improved estimate of the net influx rate K_i ($r = 0.758$, $p<0.0001$) and cerebral metabolic rate of glucose MR_{glc} ($r = 0.906$, $p<0.0001$), respectively. In conclusion, the proposed ratSUV and $ratSUV_{glc}$ provide a proxy for the K_i and MR_{glc} based on a single static [^{18}F]FDG PET SUV measurement improving clinical significance and translation of rodent studies. Given a defined strain, sex, age, diet, and weight range, this method is applicable for future experiments by converting SUV with the derived f(BW).

1. Introduction

Positron emission tomography (PET) using 2-deoxy-2–^{18}F-fluoro-D-glucose ([^{18}F]FDG) is a functional imaging tool widely applied in the neuroscience field as it allows visualization and quantitation of cerebral glucose consumption. Specifically, by applying the appropriate pharmacokinetic model, dynamic [^{18}F]FDG PET enables calculation of net influx rate (K_i) as well as the metabolic rate of glucose consumption (MR_{glc}) (Phelps et al., 1979). However, this procedure is time-consuming and invasive since arterial blood samples are required to evaluate the time course of [^{18}F]FDG concentration in arterial plasma (the arterial input function) throughout the scan. Although this procedure is feasible in rats (Hori et al., 2015; Moore et al., 2000; Shimoji et al., 2004), measuring the arterial input function without affecting the animal's physiology remains challenging. For this reason, alternative approaches using population-based (Meyer et al., 2006; Takikawa et al., 1993) or image-derived (Alf et al., 2013; Hori et al., 2015; Huang et al., 2004; Kudomi et al., 2011) input functions have been developed. Nonetheless, they still require extensive dynamic acquisitions (60–90 min), thereby considerably reducing scan throughput and they are not compatible with an awake uptake period.

These practical considerations have led researchers to shift towards simplified measures achievable using a short 10–20 min static scan after an awake uptake period. The standardized uptake value (SUV) (Huang, 2000), activity concentration divided by the injected activity per body weight (BW), represents the most often used metric. However, the major limitation of SUV (and SUV_{glc}, the SUV multiplied by plasma glucose level) is its approximative and semi-quantitative nature (Huang, 2000). As a result, the reliability of the SUV measure, especially in rodents, has been questioned (Keyes, 1995). Indeed, SUV is sensitive to several factors including, fasting duration, [^{18}F]FDG administration route, body temperature, and uptake time (Fueger et al., 2006; Schiffer et al., 2007) as these factors impact [^{18}F]FDG brain imaging in the rat (Deleye et al., 2014; Schiffer et al., 2007). An often-overlooked factor is the large weight variations (and consequent fat deposition) (Schemmel et al., 1970) that can occur over weeks and between experimental groups causing biases in the SUV measurement (Deleye et al., 2014). This is because the simple multiplicative BW factor in the SUV

* Corresponding author.
E-mail addresses: Daniele.Bertoglio@uantwerpen.be, dnl.bertoglio@gmail.com (D. Bertoglio), jeroen.verhaeghe@uantwerpen.be (J. Verhaeghe).

https://doi.org/10.1016/j.neuroimage.2021.117961
Received 21 September 2020; Received in revised form 4 February 2021; Accepted 8 March 2021
Available online 17 March 2021

does not correctly account for the impact of the varying BW on the [^{18}F]FDG brain uptake due to lower uptake in body fat compared to non-fatty tissue. Consequently, assessing whether a change in SUV or SUV_{glc} is attributed to a weight gain, disease condition, or their interaction remains extremely challenging. Similar observations have been made in human studies leading to alternative SUV calculations, where the BW in the SUV definition is replaced by lean body mass (LBM) or body surface area (BSA) (Sugawara et al., 1999). Such alternative SUV calculations could potentially be extended to small animal imaging; however, methods to estimate LBM or BSA in rats have not been developed and might be challenging.

In this study, we aim at identifying a BW-dependent conversion method for static [^{18}F]FDG PET SUV to provide an improved proxy for K_i and MR_{glc} in rats without introducing the BW-related biases as seen in the conventional SUV. As a gold standard, we first performed 60-min dynamic [^{18}F]FDG PET imaging while continuously measuring [^{18}F]FDG in arterial blood in rats with different BW. Based on theoretical approximation, we regressed a multiplicative conversion factor and used this factor to introduce ratSUV and $ratSUV_{glc}$ for which we validated their value as proxies for K_i and MR_{glc} over a large BW range.

2. Material and methods

2.1. Animals

Male Sprague Dawley rats (n = 27) (Janvier Labs, France) with different BW (200–360 g, 5–8 weeks old at time of delivery) were co-housed (3 animals/cage) in individually ventilated cages under controlled standard laboratory conditions: 12 h light/dark cycle, temperature (20–24 °C), and humidity (40–70%). Food (SSNIFF V1534–000 regular chow) and water were provided *ad libitum*, except for the fasting period before the PET scan, during which only water was accessible in cleaned cages to prevent food hoarding.

Animals were treated under the European Ethics Committee guidelines (decree 2010/63/CEE) as well as the ARRIVE guidelines, and the study protocol was approved by the Ethical Committee for Animal Testing (ECD) of the University of Antwerp, Belgium (ECD 2013–42).

2.2. [^{18}F]FDG PET acquisition and reconstruction

Small animal PET imaging was performed using two Siemens Inveon PET-CT scanners (Siemens Preclinical Solution, Knoxville, USA) (Kemp et al., 2009). On the scanning day, rats displayed a BW range of 230–487 g (approximately 6–10 weeks old). Animals were fasted starting at 18:00 of the day before the PET scan (average fasting period: 15.2 ± 3.1 h). Animal preparation and monitoring were performed as previously reported (Deleye et al., 2014). At the start of the 60-minutes PET scan, animals were injected with 33.8 ± 2.5 MBq of [^{18}F]FDG (0.6 ml) into the femoral vein via the arterio-venous shunt (see below) over a 35 s period (1 ml/min) using an infusion pump (Pump 11 Elite, Harvard Apparatus, USA). PET data were acquired in list-mode format. Following the PET scan, a 10 min CT scan was performed for attenuation correction and co-registration purposes.

Acquired PET data were reconstructed dynamically into 33 frames of increasing length (12 × 10 s, 3 × 20 s, 3 × 30 s, 3 × 60 s, 3 × 150 s, and 9 × 300 s) using 8 iterations and 16 subsets of the OSEM 3D algorithm with spatially variant resolution modeling (Miranda et al., 2020). Normalization, dead time, and CT-based attenuation corrections were applied. Since the adult rat brain size does not change over time (Mengler et al., 2014), and given the negligible contribution of scatter in FDG PET imaging of the rat brain (Konik et al., 2011; Spangler-Bickell et al., 2016) scatter correction was not included. PET image frames were reconstructed on a 128× 128×159 grid with a pixel volume of 0.776×0.776×0.796 mm^3.

2.3. [^{18}F]FDG plasma input function

Before scanning, an extracorporeal AV shunt was installed connecting the femoral artery to the ipsilateral femoral vein in series with a peristaltic pump (300 µl/min) (Weber et al., 2002) and coupled to a detector system (Twilite, Swisstrace, Switzerland) to continuously measure [^{18}F]FDG whole blood activity during the PET scan. The activity measured with the detector was decay- and background-corrected as well as cross-calibrated with the PET scanner each experimental day using a phantom scan. A biexponential function was fitted to the decaying part of the data to reduce the noise. Due to a problem with the blood measurement, one animal was omitted from the analysis.

The [^{18}F]FDG plasma fraction was determined from manual blood samples at 8 time points between 2 and 60 min p.i. in a total of 6 animals for two significantly different BW classes (range 230–234 g, 6 weeks old rats and range 396–411 g, 9 weeks old). As no difference in the plasma fraction between the low and high BW was observed (Supplementary Fig. 1) a population-based plasma fraction model was obtained by a bi-exponential fit to the average over the six animals. The [^{18}F]FDG plasma input function for each animal was generated using the individual (whole) blood activity multiplied with the population-based plasma fraction.

Glucose concentrations in whole blood and plasma were determined from manual blood samples 5 min p.i. using glucose strips in duplicate (One Touch Ultra 2, Lifescan).

2.4. Image processing and quantification

Image processing and quantification were performed in PMOD v3.6 (PMOD Technologies, Switzerland). Each PET image was transformed into the space of the Schiffer rat [^{18}F]FDG PET template (Schiffer et al., 2007) as it features several brain volume-of-interests (VOIs) which were used to extract the time-activity curves for quantification.

Kinetic modeling of the regional [^{18}F]FDG time-activity curves was performed using the standard [^{18}F]FDG irreversible 2-tissue compartment model (2TCM) (Sokoloff et al., 1977) as well as the Patlak graphical analysis (Patlak et al., 1983) using the plasma input function described above. The lumped constant (LC) was fixed at 0.71 (Tokugawa et al., 2007). From the irreversible 2TCM and Patlak model, the net influx rate (K_i, [ml/cm^3/min]) was determined, and the glucose metabolic rate (MR_{glc}, [µmol/min/100 g]) was calculated as

$$MR_{glc} = \frac{K_i \times C_p}{LC} \; x \; 100 \tag{1}$$

where C_P represents the glucose concentration in plasma and LC the lumped constant. Given the high agreement between the two methods for both K_i (r = 0.982, r^2=0.965, p<0.0001) and MR_{glc} (r = 0.991, r^2=0.983, p<0.0001), the values obtained from the Patlak plot will primarily be considered in further analysis.

In addition to the gold standard K_i and MR_{glc}, we calculated the semi-quantitative standardized uptake value (SUV), the SUV_{glc} (defined as SUV x C_P), the percent of injected activity per gram (%ID/g), and the $(\%ID/g)_{glc}$ (defined as%ID/g x C_P). All semi-quantitative values were calculated using the time interval of 50–60 min p.i.

2.5. Defining ratSUV

Using the Patlak graphical analysis of the 2TCM, we can derive an approximate relation between the true quantitative values and the static semi-quantitative measures based on body weight. [^{18}F]FDG tissue concentration C_T(t) in a pixel or VOI at later time points is approximated as (Patlak et al., 1983):

$$C_T\left(t > t^*\right) = K_i * \mathrm{AUC(t)} + VC_p(t) \tag{2}$$

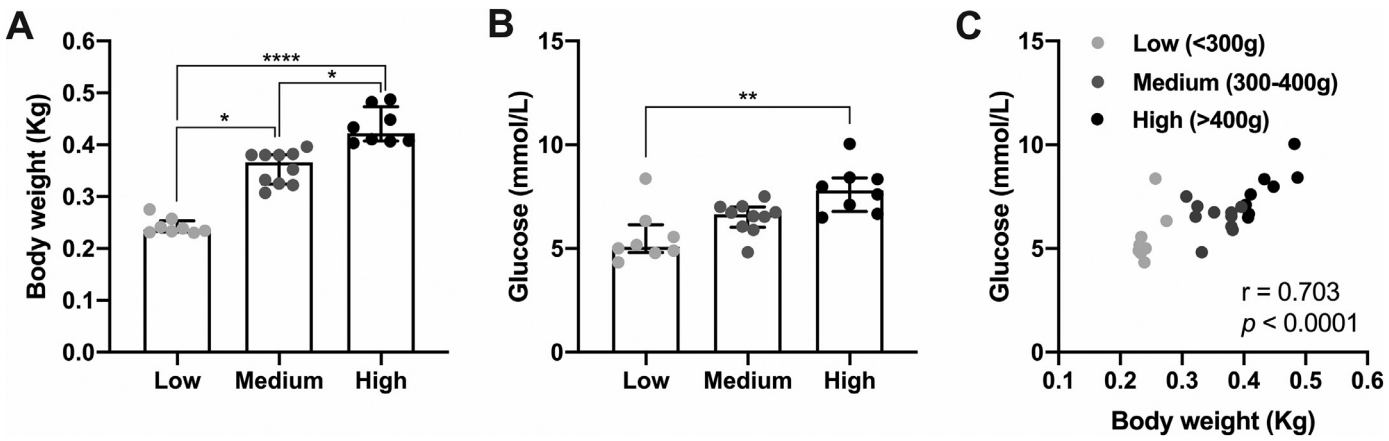

Fig. 1. Body weight and glucose measurements on [^{18}F]FDG PET acquisition day following the fasting period. (A) body weight was measured before the PET scan, while glucose levels (B) were measured 5 min post [^{18}F]FDG injection. (C) Relationship between the two variables. $^{*}p<0.05$, $^{**}p<0.01$, $^{****}p<0.0001$.

Where t* is a time point (e.g. 4 min), AUC(t) represents the area under the plasma input function ($\int_0^t C_p(\tau)d\tau$) and V accounts for the reversible compartment and the fractional blood volume.

Therefore, K_i is described as:

$$K_i = \frac{C_T(t)}{AUC(t)} - \frac{VC_p(t)}{AUC(t)} \quad (3)$$

The offset ($VC_p(t)/AUC(t)$) is region dependent (due to V) and reduces with increasing time (Supplementary Fig. 2). Thus, to derive SUV at a late time point t (e.g. 50–60 min p.i.), we can consider the following proxy for K_i by discarding the offset:

$$K_i \propto \frac{C_T(t)}{AUC(t)} \quad (4)$$

One of the main assumptions to establish the relation with SUV at time t, is that the AUC(t) is related to the injected activity (ID) per unit of BW (Huang, 2000):

$$AUC(t) \approx c \times \frac{ID}{BW} \quad (5)$$

where c is the proportionality constant at the time interval (note c is not dependent on a specific brain region). By substituting (4) and (5) and considering the SUV definition, $SUV = C_T/\frac{ID}{BW}$, we obtain:

$$\frac{1}{c}SUV \propto K_i \quad (6)$$

We hypothesize that the BW dependence of c is the main contributor to the biases seen in the SUV measurement when the body increases. Therefore, a BW dependent conversion factor is required to convert SUV to a proxy of K_i or MR_{glc}. The factor can be obtained as $1/c$ = ID/(AUCxBW), however, this requires the measurement of the plasma input function which is not readily available from a static PET scan. Therefore, we hypothesize that 1/c could be estimated from BW using a population-based quadratic regression curve (f(BW)=1/c).

Thus, by defining:

$$ratSUV = f(BW) \times SUV \propto K_i \quad (7)$$

and (cfr. (1))

$$ratSUV_{glc} = \frac{100 \times C_p}{LC} \times ratSUV \propto MR_{glc} \quad (8)$$

we obtain proxies for K_i and MR_{glc} respectively, which should be valid for a wide range of BW without introducing a weight-dependent bias. Once the relation f(BW) is established *a priori* for a rat strain, sex, and weight and age range, it can be applied to future experiments to obtain BW independent semi-quantitative proxies to K_i and MR_{glc}.

2.6. Statistical analysis

For representative purposes, animals were divided into 3 different BW classes, namely low (<0.3 kg, $n = 8$), medium (0.3–0.4 kg, $n = 10$), and high (>0.4 kg, $n = 8$). BW was measured prior to preparation for the PET scan. The Shapiro-Wilk test was used to assess the normality of the different variables. The variables K_i, MR_{glc}, ratSUV, $ratSUV_{glc}$,%ID/g, and $(\%ID/g)_{glc}$, and c passed the normality test, therefore, an ordinary one-way ANOVA with Tukey correction for multiple comparisons was used for these variables and they are reported as mean ± standard deviation (SD). The variables, BW, glucose levels, fasting duration, SUV, SUV_{glc}, and percentage offset did not pass the normality test in all groups, thus a Kruskal-Wallis test with Dunn's test to correct for multiple comparisons was applied for these variable and they are reported as median ± interquartile range (IQR). All correlations were investigated with Pearson's correlation tests, except for BW and glucose (Spearman correlation test). Finally, a quadratic function regressed 1/c as a function of the BW, as it provided better goodness of fit than a linear function. GraphPad Prism (v 8.4) was used for statistical analysis. For consistency across graphs, data are represented as median ± IQR, unless specified otherwise. All tests were two-tailed, and significance was set at $p<0.05$.

3. Results

3.1. Body weight, glucose levels, and [^{18}F]FDG plasma input function

By experimental design, BW was significantly different among the 3 categories ($p<0.0001$) (Fig. 1A). Specifically, the low BW group was 0.24±0.04 kg, the medium group was 0.37±0.05 kg, and the high BW animals were 0.42±0.06 kg. A significant difference in plasma glucose levels was also found between the low and high BW categories (low: 5.08±1.33 mmol/L, high: 7.79±1.62 mmol/L; $p = 0.0026$), while the medium group (6.64±0.99 mmol/L) did not display any significant difference (Fig. 1B). Besides, a significant relationship between BW and glucose levels was observed ($r = 0.703$, $p<0.0001$) (Fig. 1C).

[^{18}F]FDG plasma to whole blood fraction was not influenced by the BW as animals with low and high BW displayed a similar profile (Supplementary Fig. 1). Overall, [^{18}F]FDG plasma fraction decreased from 1.62±0.01 at 2 min p.i. down to 1.07±0.03 at 60 min p.i. The resulting [^{18}F]FDG plasma input function curves differed among BW categories for injected activity (Fig. 2A), SUV (Fig. 2B), or integral of the plasma input function corrected by injected activity and BW (Fig. 2C).

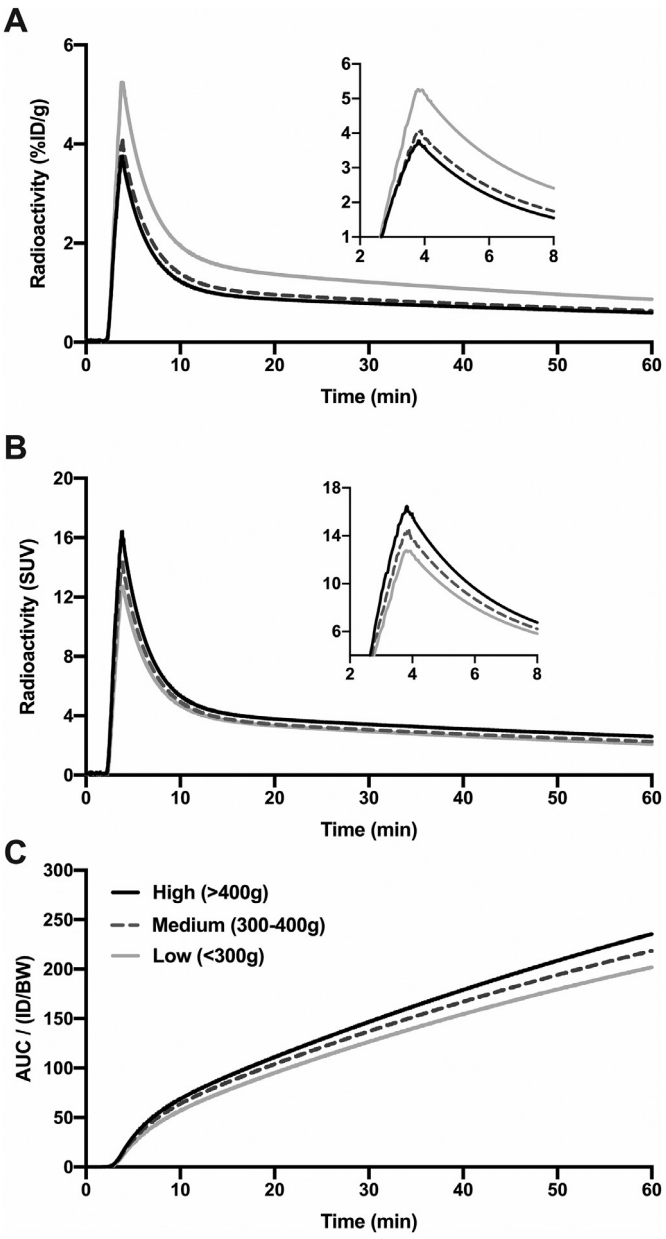

Fig. 2. Mean plasma input function curves for different BW groups following correction for injected activity (A), injected activity and BW (B), or depicted as the area under the curve (AUC) in function of time. A difference between the three groups can be appreciated in all panels despite the correction approach. BW=body weight, ID=injected activity.

3.2. [^{18}F]FDG PET quantification

[^{18}F]FDG PET data were measured both dynamically (for quantitative K_i and MR_{glc}) and statically (50–60 min) (for semi-quantitative SUV, SUV_{glc},%ID/g, and $(\%ID/g)_{glc}$) as shown in Fig. 3 for whole brain and Supplementary Fig. 3 for cortex, hippocampus, thalamus, and caudate putamen. No difference in the net [^{18}F]FDG influx rate K_i was measured among the 3 investigated BW groups for the whole brain (Low: 0.020±0.003 ml/cm^3/min, Medium: 0.019±0.004 ml/cm^3/min, High: 0.017 ± 0.005 ml/cm^3/min; $F_{(2,23)}$=1.702, p = 0.204) (Fig. 3A). On the contrary, the metabolic rate of glucose MR_{glc} differed (Low: 13.1 ± 4.9 µmol/min/100 g, Medium: 17.5 ± 3.6 µmol/min/100 g, High: 18.4 ± 3.7 µmol/min/100 g; $F_{(2,23)}$=5.275, p = 0.013) (Fig. 3B) with a significant difference between the low and high BW groups (p = 0.0125).

The differences in BW among the 3 categories affected the semi-quantitative measurements resulting in conflicting data dependent on the metric used. Indeed, SUV increased with BW (Low: 2.4 ± 0.2, Medium: 2.7 ± 0.3, High: 2.8 ± 0.3; p = 0.0135) with a significant difference between the low and high groups (p = 0.0148) (Fig. 3C). Similarly, SUV_{glc} increased with BW (Low: 12.8 ± 6.5, Medium: 18.4 ± 2.5, High: 23.3 ± 5.1; p = 0.0042) with an overestimated significant difference between the low and high BW groups (p = 0.0029) (Fig. 3D). On the other hand, %ID/g decreased with higher BW (Low: 1.03 ± 0.13%, Medium: 0.79 ± 0.18%, High: 0.66 ± 0.13%; $F_{(2,23)}$=33.49, p<0.0001) (Fig. 3E), while $(\%ID/g)_{glc}$ did not result in any difference (Low: 5.4 ± 2.2%, Medium: 4.7 ± 1.3%, High: 5.0 ± 1.1%; $F_{(2,23)}$=0.885, p = 0.42) (Fig. 3F).

3.3. Body weight influences the conversion factor c

In line with our hypothesis, the factor c was different among BW categories (Low: 107.8 ± 16.0 g/min*mL, Medium: 120.4 ± 9.8 g/min*mL, High: 138.0 ± 31.5 g/min*mL; $F_{(2,23)}$=8.638, p = 0.0016) (Fig. 4A) with a significant difference between the low and high groups (p = 0.0013) as well as the medium and high groups (p = 0.0254).

Importantly, as postulated in Eq. (6), dividing SUV and SUV_{glc} by the factor c resulted in a simplified measure for K_i and MR_{glc}, respectively, as demonstrated by the highly significant correlations between SUV/c vs K_i (r = 0.979, r^2=0.96, p<0.0001, Fig. 4B) and SUV_{glc}/c vs MR_{glc} (r = 0.960, r^2=0.92, p<0.0001, Fig. 4C).

3.4. RatSUV and ratSUV$_{glc}$ are proxies for K_i and MR$_{glc}$

Using the measured conversion factor c values, the regression 1/c in function of BW was determined based on a quadratic function f(BW) (r^2=0.697) as shown in Fig. 5 and described as follows:

$$f(BW) = -0.04425 * BW^2 + 0.02015 * BW + 0.006944 \quad (9)$$

Where BW is the BW of the animal.

While SUV did not correlate with K_i (r = 0.228, r^2=0.05, p = 0.263), the ratSUV resulted in a good agreement (r = 0.758, r^2=0.57, p<0.0001) (Figs. 6A and 6B). Similarly, although SUV_{glc} correlated with MR_{glc} (r = 0.818, r^2=0.67, p<0.0001), the slope of the regression was biased (slope=1.56) (Fig. 6C). On the contrary, the $ratSUV_{glc}$ resulted in a stronger correlation (r = 0.906, r^2=0.82, p<0.0001) without affecting the slope of the regression (slope=1.00) (Fig. 6D). Analysis of individual brain regions resulted in the same outcome as shown in Supplementary Figs. 4 and 5 and summarized in Supplementary Tables 1 and 2 for K_i and MR_{glc}, respectively.

4. Discussion

The commonly applied semi-quantitative metrics SUV and SUV_{glc} assume a linear multiplicative BW factor that does not correctly account for the impact of the varying [^{18}F]FDG uptake in body fat compared to non-fatty tissue. This effect is magnified when large weight variations occur over weeks and between experimental groups causing biases in the semi-quantitative metrics. Male Sprague Dawley rats can almost double their weight (from 250 g to 450 g) in just five weeks (Janvier). In this scenario, it is difficult to assess whether a change in SUV or SUV_{glc} measurement is attributed to weight gain, disease condition, or their interaction. This study focused on the identification of a conversion method for improved [^{18}F]FDG PET quantification based on simple and high-throughput static acquisition in rats. We determined a quadratic function f(BW) that can be applied to future rat experiments to convert SUV and SUV_{glc}, obtained in the time interval 50–60 min p.i., by multiplying for f(BW) as described in Eq. (9) for more stable and accurate estimation of K_i and MR_{glc}. Accordingly, the derived ratSUV and $ratSUV_{glc}$ respectively outperformed the semi-quantitative SUV, SUV_{glc},%ID/g, and $(\%ID/g)_{glc}$, unable to correctly reflect K_i and MR_{glc}.

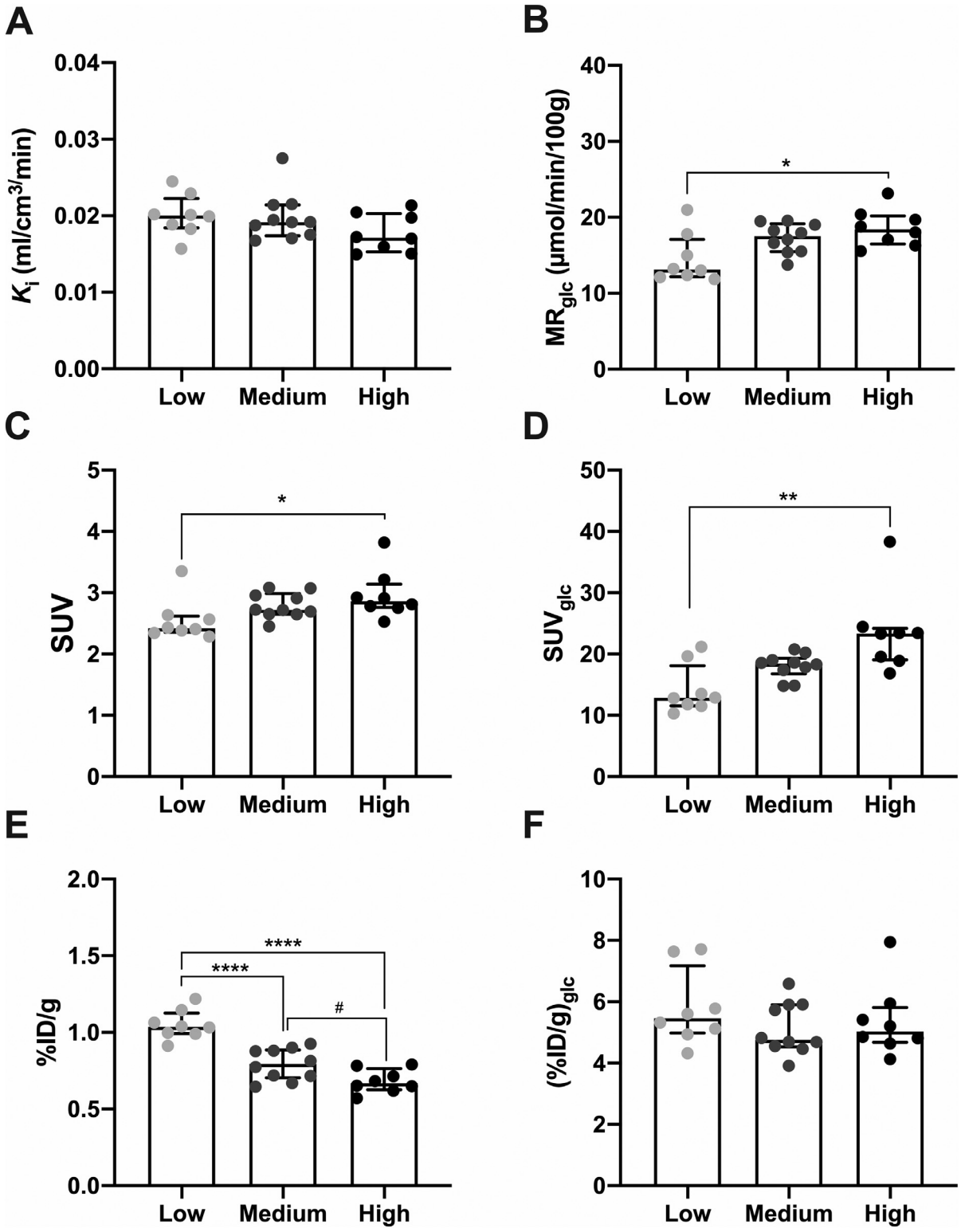

Fig. 3. Overview of [^{18}F] FDG PET measurements for the whole brain. The net [^{18}F]FDG influx rate K_i (A) and the metabolic rate of glucose MR_{glc} (B) are quantitative measurements and based on dynamic data with the plasma input function. SUV (C), SUV_{glc} (D),%ID/g (E), and $(\%ID/g)_{glc}$ (F) are semi-quantitative (static) approaches based on the time interval 50 to 60 min post-injection. Note the quantification discrepancies between the static and dynamic measures. $^{\#}p = 0.051$, $^{*}p<0.05$, $^{**}p<0.01$, $^{****}p<0.0001$.

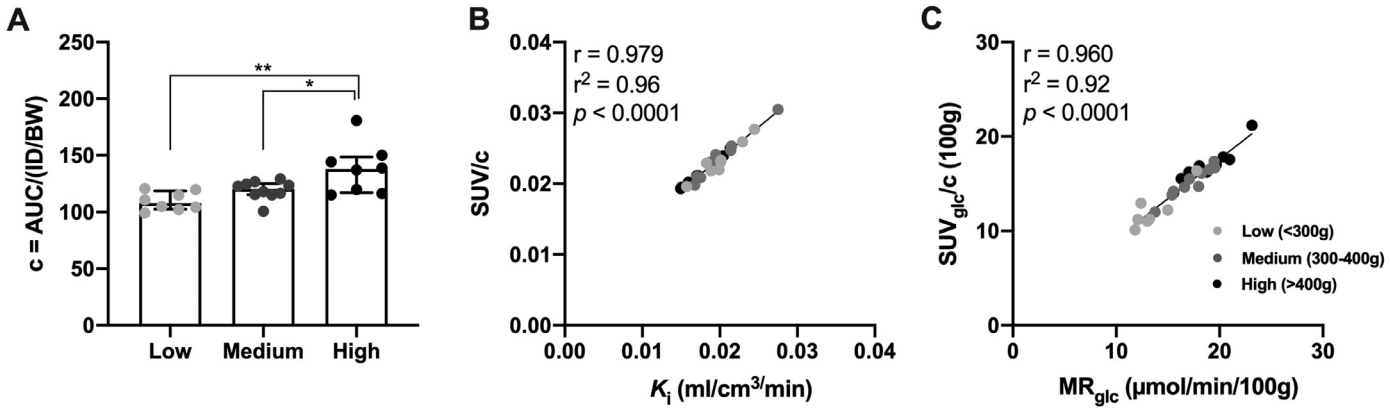

Fig. 4. Measurement of the conversion factor c. (A) The conversion factor c significantly differs among body weight groups. SUV and SUVglc divided by c highly correlate with K_i (B) and MR_{glc} (C), respectively. Thus, by applying the inverse of c to SUV and SUV_{glc} according to Eqs. (7) and 8, it is possible to provide a simplified measure for K_i and MR_{glc}. $^{*}p<0.05$, $^{**}p<0.01$.

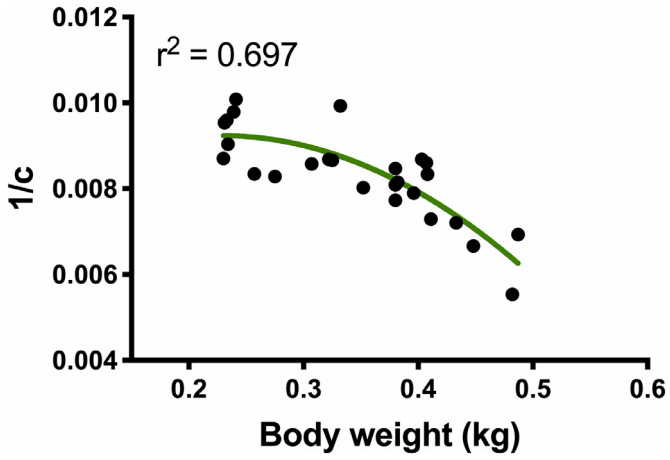

Fig. 5. Relationship of the conversion factor c in function of body weight. Based on the measured conversion factor c values, a quadratic function was obtained from the regression of the data as described in Eq. (9). This function can be used to estimate the conversion factor c, ratSUV, and $ratSUV_{glc}$. The quadratic function is shown in grey.

In this study, we found that differences in BW are associated with alterations in the plasma glucose levels. This relationship has been previously reported both in rodents (Chang et al., 2015) as well as in humans (Sepp et al., 2014; Walsh et al., 2018). Noteworthy, SUV_{glc} correlated with MR_{glc}, although introducing an overestimation (slope = 1.56), while SUV did not show an association with K_i. By correcting SUV for the plasma glucose levels (which is associated with BW) the proportionality of fatty/non-fatty tissue is partially taken into account. Nevertheless, the application of the quadratic function f(BW) always improved the relationship to MR_{glc}.

When performing small animal dynamic PET imaging, animals must be anesthetized during the whole scan duration, including the initial period following [^{18}F]FDG injection. The resulting reduced cerebral glucose under anesthesia (Shimoji et al., 2004) does not hamper the findings of the present study as the correction method is brain uptake independent. Additionally, Hori and colleagues reported the AUCs of the input functions between awake and anesthetized rats to be comparable (Hori et al., 2015). Since the correction method proposed is based on AUC, BW, and injected activity, it is applicable for both anesthetized and awake studies.

The main advantage of the presented method is that only the BW is required to convert SUV to ratSUV for [^{18}F]FDG quantification once the relationship for a species, strain, sex, weight range, and scan interval has been established in a preceding dynamic experiment, which is only to be performed once. While we demonstrated its applicability for [^{18}F]FDG, such a method might be extended to other radiotracers with an irreversible binding that can be modeled with the Patlak graphical analysis.

Since there is an offset in the estimation of K_i from the Patlak method as described in Eq. (3) and SUV/c (Eq. (6)), the choice of the time interval is relevant. As the offset is uptake dependent, it will vary in each experimental design (e.g. awake, anesthetized, fasted, disease condition, brain region) and it cannot be estimated without measurement of the arterial input function and dynamic acquisition. However, the offset reduces with time (Supplementary Fig. 2), therefore, if later time intervals are used, its impact on the relationship between ratSUV and K_i is limited.

Alternatively to the presented method, [^{18}F]FDG tissue uptake may be corrected with the use of a blood sample, by choosing between two approaches: (i) scaling an average input function curve (Hori et al., 2015) to be used in the kinetic analysis or (ii) normalizing a static uptake measure by one sample (Hunter et al., 1996; Schiffer et al., 2007). However, scaling an average curve still requires the generation of a population-based characterization due to the differences in input function when large BW variations are present. Besides, it retains the need for an extensive dynamic PET acquisition. Otherwise, normalizing by one plasma sample would not be a critical limitation under anesthetized condition, however, awake PET imaging in small animals is becoming a reality (Miranda et al., 2019a, 2019b) and the need for a blood sample during an awake PET acquisition would be extremely challenging to reconcile without inducing stress in the animal.

A common alternative to SUV quantification to eliminate the weight dependence considers SUV ratios, i.e. SUV in a VOI divided by SUV in a reference region. However, this method is critically dependent on the existence of a brain region not affected across experimental groups (reference region), an assumption difficult to validate *a priori* and which is known not to apply to many disease models.

We observed a significant difference in MR_{glc} between low and high BW groups even though cerebral MR_{glc} is regulated to remain at a rather constant rate. While it is unlikely that the MR_{glc} difference was due to the lumped constant in the range of measured plasma glucose concentration levels (Schuier et al., 1990), a possible reason could be a maturation effect. Indeed, the different weight classes reflected different ages as the rats of the low and high weight groups were respectively 6 and 10 weeks of age. In humans and non-human primates, the cerebral MR_{glc} increases steadily from low values in infants to a maximum between 4 and 12 years (Herholz et al., 2004; Kinnala et al., 1996). Thus, it is

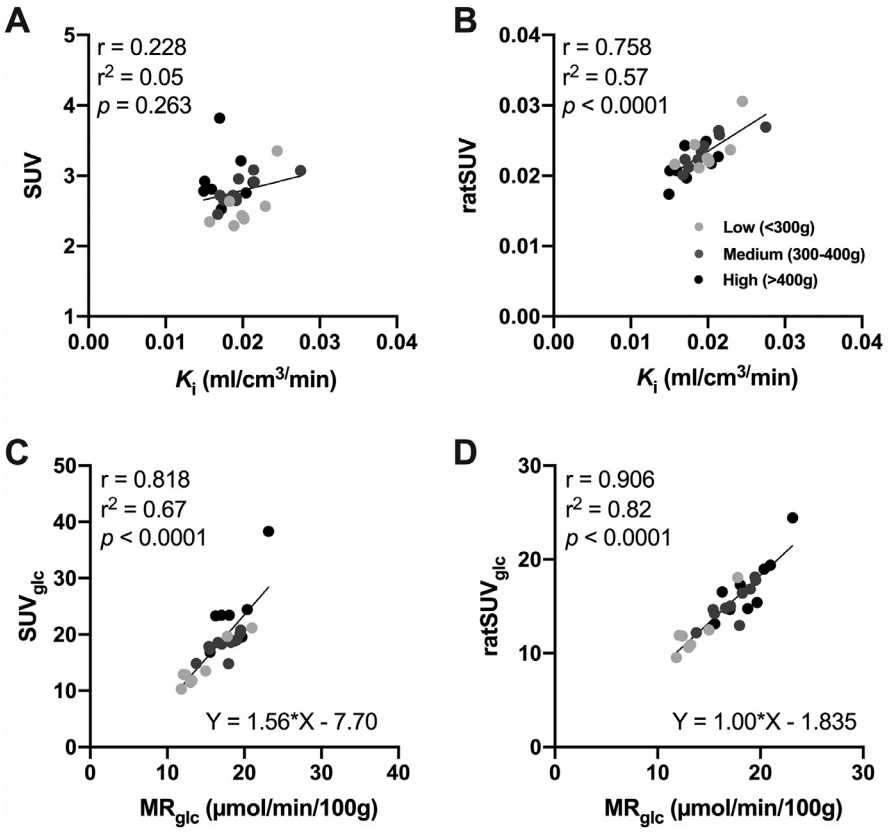

Fig. 6. Relationship between semi-quantitative static and quantitative dynamic measurements for [^{18}F] FDG. While SUV does not correlate with the net influx rate K_i (A), multiplying SUV for the factor f(BW) described in Eq. (9) provides a significant correlation with K_i (B). Similarly, while SUV_{glc} is associated with the metabolic glucose rate MR_{glc} (C), conversion of SUV_{glc} for the factor f(BW) as described in Eq. (9) improves the estimation of MR_{glc} (D). Whole brain values are reported.

conceivable that a similar MR_{glc} increase is present among the different BW categories.

5. Conclusion

This study determined a quadratic function f(BW) dependent on body weight that converts the semi-quantitative measures SUV and SUV_{glc} during the time interval 50–60 min p.i to proxies of K_i and MR_{glc}. Given a defined strain, sex, age, diet, and weight range, this quadratic function f(BW) can be applied to all future rat experiments to correct SUV and SUV_{glc} based on a single static [^{18}F]FDG PET scan to estimate K_i and MR_{glc} noninvasively.

Declaration of Competing Interest

The authors declare no competing interest.

Acknowledgements

We thank Philippe Joye for his valued technical assistance.

Funding

DB is supported by a post-doctoral fellowship from the Research Foundation Flanders (FWO, 1229721N). This work was supported by the University of Antwerp, Belgium through a postdoctoral research position for SD, an associate professor position for JV, and a full professor position for StS as well as SiS. SiS is also supported by Antwerp University Hospital, Belgium through a departmental position. Hardware and experimental costs were funded by a BOF KP (FFB140088) of the University of Antwerp.

Data and code availability statement

Data are available upon reasonable request to the corresponding author through a data sharing agreement.

CRediT Author Contribution Statement

Daniele Bertoglio: Formal analysis; Methodology; Validation; Visualization; Writing - original draft; Writing - review & editing. **Steven Deleye:** Conceptualization; Funding acquisition; Formal analysis; Methodology; Writing - review & editing. **Alan Miranda:** Software; Writing - review & editing. **Sigrid Stroobants:** Resources, Writing - review & editing. **Steven Staelens:** Conceptualization; Resources; Writing - review & editing. **Jeroen Verhaeghe:** Conceptualization; Funding acquisition; Formal analysis; Validation; Visualization; Writing - original draft; Writing - review & editing.

Supplementary materials

Supplementary material associated with this article can be found, in the online version, at doi:10.1016/j.neuroimage.2021.117961.

References

Alf, M.F., Wyss, M.T., Buck, A., Weber, B., Schibli, R., Kramer, S.D., 2013. Quantification of brain glucose metabolism by 18F-FDG PET with real-time arterial and image-derived input function in mice. J. Nucl. Med. 54, 132–138.

Chang, R.C., Shi, L., Huang, C.C., Kim, A.J., Ko, M.L., Zhou, B., Ko, G.Y., 2015. High-fat diet-induced retinal dysfunction. Invest. Ophthalmol. Vis. Sci. 56, 2367–2380.

Deleye, S., Verhaeghe, J., wyffels, L., Dedeurwaerdere, S., Stroobants, S., Staelens, S., 2014. Towards a reproducible protocol for repetitive and semi-quantitative rat brain imaging with (18) F-FDG: exemplified in a memantine pharmacological challenge. Neuroimage 96, 276–287.

Fueger, B.J., Czernin, J., Hildebrandt, I., Tran, C., Halpern, B.S., Stout, D., Phelps, M.E., Weber, W.A., 2006. Impact of animal handling on the results of 18F-FDG PET studies in mice. J. Nucl. Med. 47, 999–1006.

Herholz, K., Herscovitch, P., Heiss, W., 2004. NeuroPET - Positron Emission Tomography in Neuroscience and Clinical Neurology. Springer-Verlag Berlin Heidelberg.
Hori, Y., Ihara, N., Teramoto, N., Kunimi, M., Honda, M., Kato, K., Hanakawa, T., 2015. Noninvasive quantification of cerebral metabolic rate for glucose in rats using (18)F-FDG PET and standard input function. J. Cereb. Blood Flow Metab. 35, 1664–1670.
Huang, S.C., 2000. Anatomy of SUV. Standardized uptake value. Nucl. Med. Biol. 27, 643–646.
Huang, S.C., Wu, H.M., Shoghi-Jadid, K., Stout, D.B., Chatziioannou, A., Schelbert, H.R., Barrio, J.R., 2004. Investigation of a new input function validation approach for dynamic mouse microPET studies. Mol. Imaging Biol. 6, 34–46.
Hunter, G.J., Hamberg, L.M., Alpert, N.M., Choi, N.C., Fischman, A.J., 1996. Simplified measurement of deoxyglucose utilization rate. J. Nucl. Med. 37, 950–955.
Janvier, L., Sprague Dawley® Rat.
Kemp, B.J., Hruska, C.B., McFarland, A.R., Lenox, M.W., Lowe, V.J., 2009. NEMA NU 2-2007 performance measurements of the Siemens Inveon preclinical small animal PET system. Phys. Med. Biol. 54, 2359–2376.
Keyes, J.W., 1995. SUV: standard uptake or silly useless value? J. Nucl. Med. 36, 1836–1839.
Kinnala, A., Suhonen-Polvi, H., Aarimaa, T., Kero, P., Korvenranta, H., Ruotsalainen, U., Bergman, J., Haaparanta, M., Solin, O., Nuutila, P., Wegelius, U., 1996. Cerebral metabolic rate for glucose during the first six months of life: an FDG positron emission tomography study. Arch. Dis. Child Fetal Neonatal. Ed. 74, F153–F157.
Konik, A., Koesters, T., Madsen, M.T., Sunderland, J.J., 2011. Evaluation of attenuation and scatter correction requirements as a function of object size in small animal PET imaging. IEEE Trans. Nucl. Sci. 58, 2308–2314.
Kudomi, N., Bucci, M., Oikonen, V., Silvennoinen, M., Kainulainen, H., Nuutila, P., Iozzo, P., Roivainen, A., 2011. Extraction of input function from rat [18F]FDG PET images. Mol. Imaging Biol. 13, 1241–1249.
Mengler, L., Khmelinskii, A., Diedenhofen, M., Po, C., Staring, M., Lelieveldt, B.P., Hoehn, M., 2014. Brain maturation of the adolescent rat cortex and striatum: changes in volume and myelination. Neuroimage 84, 35–44.
Meyer, P.T., Circiumaru, V., Cardi, C.A., Thomas, D.H., Bal, H., Acton, P.D., 2006. Simplified quantification of small animal [18F]FDG PET studies using a standard arterial input function. Eur. J. Nucl. Med. Mol. Imaging 33, 948–954.
Miranda, A., Bertoglio, D., Glorie, D., Stroobants, S., Staelens, S., Verhaeghe, J., 2020. Validation of a spatially variant resolution model for small animal brain PET studies. Biomed. Phys. Eng. Express 6, 045001.
Miranda, A., Glorie, D., Bertoglio, D., Vleugels, J., De Bruyne, G., Stroobants, S., Staelens, S., Verhaeghe, J., 2019a. Awake (18)F-FDG PET imaging of memantine-induced brain activation and test-retest in freely running mice. J. Nucl. Med. 60, 844–850.
Miranda, A., Kang, M.S., Blinder, S., Bouhachi, R., Soucy, J.P., Aliaga-Aliaga, A., Massarweh, G., Stroobants, S., Staelens, S., Rosa-Neto, P., Verhaeghe, J., 2019b. PET imaging of freely moving interacting rats. Neuroimage 191, 560–567.
Moore, A.H., Osteen, C.L., Chatziioannou, A.F., Hovda, D.A., Cherry, S.R., 2000. Quantitative assessment of longitudinal metabolic changes in vivo after traumatic brain injury in the adult rat using FDG-microPET. J. Cereb. Blood Flow Metab. 20, 1492–1501.
Patlak, C.S., Blasberg, R.G., Fenstermacher, J.D., 1983. Graphical evaluation of blood--to-brain transfer constants from multiple-time uptake data. J. Cereb. Blood Flow Metab. 3, 1–7.
Phelps, M.E., Huang, S.C., Hoffman, E.J., Selin, C., Sokoloff, L., Kuhl, D.E., 1979. Tomographic measurement of local cerebral glucose metabolic rate in humans with (F-18)2-fluoro-2-deoxy-D-glucose: validation of method. Ann. Neurol. 6, 371–388.
Schemmel, R., Mickelsen, O., Mostosky, U., 1970. Influence of body weight, age, diet and sex on fat depots in rats. Anat. Rec. 166, 437–445.
Schiffer, W.K., Mirrione, M.M., Dewey, S.L., 2007. Optimizing experimental protocols for quantitative behavioral imaging with 18F-FDG in rodents. J. Nucl. Med. 48, 277–287.
Schuier, F., Orzi, F., Suda, S., Lucignani, G., Kennedy, C., Sokoloff, L., 1990. Influence of plasma glucose concentration on lumped constant of the deoxyglucose method: effects of hyperglycemia in the rat. J. Cereb. Blood Flow Metab. 10, 765–773.
Sepp, E., Kolk, H., Loivukene, K., Mikelsaar, M., 2014. Higher blood glucose level associated with body mass index and gut microbiota in elderly people. Microb. Ecol. Health Dis. 25.
Shimoji, K., Ravasi, L., Schmidt, K., Soto-Montenegro, M.L., Esaki, T., Seidel, J., Jagoda, E., Sokoloff, L., Green, M.V., Eckelman, W.C., 2004. Measurement of cerebral glucose metabolic rates in the anesthetized rat by dynamic scanning with 18F-FDG, the ATLAS small animal PET scanner, and arterial blood sampling. J. Nucl. Med. 45, 665–672.
Sokoloff, L., Reivich, M., Kennedy, C., Des Rosiers, M.H., Patlak, C.S., Pettigrew, K.D., Sakurada, O., Shinohara, M., 1977. The [14C]deoxyglucose method for the measurement of local cerebral glucose utilization: theory, procedure, and normal values in the conscious and anesthetized albino rat. J. Neurochem. 28, 897–916.
Spangler-Bickell, M.G., de Laat, B., Fulton, R., Bormans, G., Nuyts, J., 2016. The effect of isoflurane on (18)F-FDG uptake in the rat brain: a fully conscious dynamic PET study using motion compensation. EJNMMI Res. 6, 86.
Sugawara, Y., Zasadny, K.R., Neuhoff, A.W., Wahl, R.L., 1999. Reevaluation of the standardized uptake value for FDG: variations with body weight and methods for correction. Radiology 213, 521–525.
Takikawa, S., Dhawan, V., Spetsieris, P., Robeson, W., Chaly, T., Dahl, R., Margouleff, D., Eidelberg, D., 1993. Noninvasive quantitative fluorodeoxyglucose PET studies with an estimated input function derived from a population-based arterial blood curve. Radiology 188, 131–136.
Tokugawa, J., Ravasi, L., Nakayama, T., Schmidt, K.C., Sokoloff, L., 2007. Operational lumped constant for FDG in normal adult male rats. J. Nucl. Med. 48, 94–99.
Walsh, E., Burns, R., Abhayaratna, W., Anstey, K., Cherbuin, N., 2018. Physical activity and blood glucose effects on weight gain over 12 years in middle-aged adults. J. Obesity Chronic Dis. 2, 20–25.
Weber, B., Burger, C., Biro, P., Buck, A., 2002. A femoral arteriovenous shunt facilitates arterial whole blood sampling in animals. Eur. J. Nucl. Med. Mol. Imaging 29, 319–323.